complete new version of AL's Table 3 is shown which was calculated with the analytical-method program and $\Delta\mu = 0{\cdot}0001$. In relation to the last two columns in AL's Table 3, it should be pointed out that AL's equation (6) should read

$$P_n = 0{\cdot}5[(\cos^2\beta + \sin^2\beta\cos^2\alpha) + (\sin^2\beta + \cos^2\beta\cos^2\alpha)\cos^{2n}2\theta].$$

It was decided that more tests would be desirable for the four-circle diffractometer geometry. Hence we also carried out AL's irregular crystal test for (1) values of μ = 0·01, 0·1, 1·0, 10·0 and 100·0 and (2) for the reflections 1 2 3 and 1 −2 −3, μ = 1·0, for azimuthal angles in the range 0 to 360° calculated in steps of 10°. A resumé of the values obtained is given in Tables 6 and 7. Positive ψ corresponds to an anti-clockwise rotation when looking along the normal to the reflecting plane towards the crystal. $\psi = 0$ is defined by the bisecting position of $\omega = \theta$. As a help for checking programs we give in Table 8 directional components of unit vectors in the direction of the incident and reflected beams. These components are with respect to the direct crystal axes. Another useful check on a program is the volume calculated for the crystal. These values are given in Table 9.

AL's regular crystal test

We obtained the same values as in AL's Table 2. Our complete results may be found in the Supplementary Publication.

We thank Professor D. Templeton and Dr L. Templeton for having confirmed the results of some of the tests by running them with their own analytical-method program.

References

ALCOCK, N. W. (1970). *Crystallographic Computing*, edited by F. R. AHMED, pp. 271–278. Copenhagen: Munksgaard.
ALCOCK, N. W. (1974). *Acta Cryst.* A**30**, 332–335.
BUSING, W. R. & LEVY, H. A. (1957). *Acta Cryst.* **10**, 180–182.
CAHEN, D. & IBERS, J. A. (1972). *J. Appl. Cryst.* **5**, 298–299.
CAHEN, D. & IBERS, J. A. (1973). *J. Appl. Cryst.* **6**, 244.
EVANS, H. T. (1952). *J. Appl. Phys.* **23**, 663–668.
MEULENAER, J. DE & TOMPA, H. (1965). *Acta Cryst.* **19**, 1014–1018.
STEWART, J. M. (1976). XRAY System. Rep. TR-446 of the Computer Science Center, University of Maryland, College Park, Maryland, USA.

Acta Cryst. (1980). A**36**, 686–696

The Critical-Voltage Effect in Convergent-Beam High-Voltage Electron Diffraction

BY J. R. SELLAR,* D. IMESON† AND C. J. HUMPHREYS

University of Oxford, Department of Metallurgy and the Science of Materials, Parks Road, Oxford OX1 3PH, England

(*Received* 21 *July* 1979; *accepted* 22 *February* 1980)

Abstract

The critical-voltage effect has been combined with the convergent-beam electron diffraction technique using a high-voltage electron microscope. The method allows the critical voltage V_c to be detected to within approximately ±1 kV, compared with ±5 kV in previous methods. This accuracy is achievable throughout the 100 to 1000 kV accelerating-voltage range of the high-voltage microscope used. V_c has also been determined by varying the specimen temperature at constant voltage, which has the advantage that all electron-optical parameters are kept constant: thus the 'transfer function' of the microscope is constant. The critical voltage is easily identified experimentally by the appearance of a characteristic 'dark band' in the Bragg-satisfied second-order convergent-beam disc. Changes in the asymmetry of the Kikuchi line within the dark band enable the precise localization of V_c to ±1 kV to be made. The improved precision of this new method considerably increases its application to the determination of scattering factors in pure materials and to ordering and electron-transfer effects in certain alloys. The method is illustrated by applying it to Cu and Cu–Al alloys.

* Present address: Research School of Chemistry, Australian National University, Canberra, ACT 2600, Australia.
† Present address: Department of Materials Science and Engineering, MIT, Cambridge, Massachusetts 02139, USA.

0567-7394/80/040686-11$01.00

1. Introduction

If a crystal is set at a Bragg-reflecting position, the diffracted beam intensity is usually strong owing to the constructive interference of waves scattered in the diffracted beam direction. However, for a particular electron accelerating voltage, known as the critical voltage, V_c, the diffracted beam intensity is very small, due to destructive rather than constructive interference. The critical voltage is very sensitive to the low-order Fourier coefficients of the crystal potential, V_g, and hence it can be used to determine these and related quantities (*e.g.* scattering factors and charge densities). Such quantities can alternatively be determined from convergent-beam (CB) diffraction experiments. The critical-voltage method is in general slightly more accurate (see Goodman, 1978), with both methods yielding V_g values to 1% or better.

The utility of the experimentally determined scattering factors depends entirely upon the precision of the measurements. Differences between charge densities (or scattering factors or potentials) in a crystal and in a free atom are usually very small, and although these differences can be detected for many monatomic solids, using critical-voltage or CB techniques, further precision in these measurements is highly desirable (see Smart & Humphreys, 1978). In principle, the critical-voltage effect can be used in the study of ordering in alloys (Lally, Humphreys, Metherell & Fisher 1972). However, although results have been obtained in a few cases (Kuroda, Tomokiyo & Eguchi, 1978; Butler, 1972; Thomas, Shirley, Lally & Fisher, 1974), in other cases the degree of short-range order could not be estimated accurately owing to the inadequate experimental sensitivity (Kuroda, Tomokiyo & Eguchi, 1977; Sinclair, Goringe & Thomas, 1975).

The object of this paper is to investigate the application of a method that combines the convergent-beam technique and the critical-voltage effect. It will be shown that this method is considerably more accurate than either technique used separately. The method is reliably and routinely available on at least one type of microscope (the AEI EM7) without modification of the microscope column or specimen position. The method will be illustrated by applying it to copper and to Cu–Al alloys. In this work, a new technique of determining the critical voltage by varying the specimen temperature rather than the electron-accelerating voltage is also proposed.

2. Convergent-beam and critical-voltage methods

In order to understand the combined technique, it is necessary first to consider the individual CB and V_c methods.

(*a*) *Convergent-beam diffraction*

A convergent cone of incident electrons is focused to a small cross-over at the specimen. The convergent incident beam results in the usual diffracted beam spots being spread into circular discs. Each point in a disc corresponds to a particular angle of incidence, so that the variation of intensity across each disc represents the variation in intensity in each diffracted beam as a function of the angle of incidence, *i.e.* a 'rocking curve'. Accurate scattering factors have been determined by comparing experimental convergent-beam discs with those calculated by *n*-beam dynamical theory (Goodman & Lehmpfuhl, 1967; Goodman, 1976). For summaries of recent developments at voltages around 100 kV see Lehmpfuhl (1978) and Cowley (1978).

At higher voltages a few CB studies have been made (Smith & Cowley, 1971; Steeds, Jones, Rackham & Shannon, 1976; Rackham & Rickards, 1977), but there have been difficulties in obtaining sufficiently small electron-beam-spot sizes for good patterns. The present work is based on our previous experience in which CB patterns have been obtained in an instrument operating at 1 MV with a spot size of approximate radius 500 Å deteriorating to 1000 Å at 400 kV. An angular resolution of 10^{-4} rad was obtained at 1 MV (Moodie, Sellar, Imeson & Humphreys, 1977; Moodie, Humphreys, Imeson & Sellar, 1978).

(*b*) *The critical-voltage effect*

At the critical voltage a sharp extinction effect, or change in symmetry, is observed in the diffraction spots, rocking curves, zone-axis patterns, extinction contours and second- or higher-order Kikuchi lines. The V_c effect and its applications are discussed by Nagata & Fukuhara (1967), Watanabe, Uyeda & Kogiso (1968) and Lally, Humphreys, Metherell & Fisher (1972). The basic theory will be outlined in §4.

Accuracies of 0·2 and 0·6% in the determination of V_{111} in Si and Ge respectively have been reported using the critical-voltage method (Hewat & Humphreys, 1974) and 0·3% accuracy has been claimed for the determination in Ge by a comparison of V_c results, using a 1 MV HVEM, with CB results, using a microscope operating at 100 kV (Shishido & Tanaka, 1976). The total error in estimating V_c is usually at best ± 5 kV, derived from interpolation over observations 5 kV apart, and averaging over several sets of data (Hewat, 1975).

(*c*) *Convergent-beam critical-voltage measurements*

Attempts at some form of combination of the two techniques have been made (Bell, 1971; Butler, 1972, 1973; Hewat & Humphreys, 1974) but have failed to obtain CB patterns showing fine detail, a consequence of the large (roughly 1 μm) spot sizes used. In these

previous investigations an accuracy of approximately ± 5 kV was obtained for the measurement of V_c. In the present study, using smaller spot sizes and hence higher-quality CB patterns, an observational accuracy of about ± 1 kV in detecting V_c was obtained.

3. Experimental procedures

(*a*) *Convergent-beam mode of operation*

A convergent electron beam is obtained in the EM7 HVEM by operating the first condenser lens in saturation and using the second condenser to transfer the image of the cross-over onto the specimen. (Other microscopes, without the particularly strong first condenser lens of the EM7, may require an additional pre-specimen lens to achieve a small spot size. Alternatively, the pre-field of the objective lens might be used.) To reduce the spot size further, the Wehnelt bias voltage is increased and the filament desaturated. The diffraction pattern obtained then consists of a number of convergent-beam diffraction discs, as in Fig. 1(*a*) for example, each point in the disc corresponding to a particular angle of incidence in a cone whose half angle is determined by the particular condenser aperture size.

Small amounts of defocus in the second condenser lens produce images of the specimen in each of the discs, which are inverted on passing through focus, as the cross-over passes through the specimen. This property is used initially to focus the CB pattern. A sensitive image intensifier was used to display the pattern, at the highest camera lengths utilized.

In the experiments on copper and its aluminium alloys, no degradation of the CB pattern due to radiation damage was observed. Contamination problems were avoided partly because, as a part of the experiment, the specimen was heated, but they are anyway less severe at 300 kV than as previously reported at 1 MeV (Moodie, Sellar, Imeson & Humphreys, 1977) because of the larger spot size, room-temperature operation being possible for quite long periods.

(*b*) *Materials and specimen preparation*

The materials used in the present experiments were zone-refined copper (supplied by Australian Mineral Development Laboratories) and single crystals of α-CuAl alloys containing 5·03, 11·50 and 16·73 at. % aluminium. There are two accessible critical voltages (for 222 and 400 reflections respectively) in these materials, high-quality specimens could be prepared and several V_c-effect studies by other methods already exist with which experimental results may be compared (*e.g.* Hewat, 1975; Arii, Uyeda, Terasaki & Watanabe, 1973; Kuroda, Tomokiyo & Eguchi, 1977). The more concentrated CuAl alloys are also known to exhibit a tendency to short-range order (*e.g.* Epperson, Fürnrohr & Ortiz, 1978).

Preparation for electron microscopic examination was achieved using a jet electropolish to indent disc-shaped specimens and a slow final electropolish to perforation in 33% nitric acid in methanol at very low temperature. Specimens could, with care, be produced almost free of bends, with clean, flat surfaces, and with an even, symmetric thickness profile showing a wedge angle of about 10^{-2} rad over large areas. It is important to emphasize that such high-quality specimens are essential if CB patterns showing fine detail are to be obtained with the spot size used.

(*c*) *Techniques of critical-voltage measurement*

The identification of the critical voltage in the selected-area, parallel-illumination diffraction mode of the HVEM is usually made at a fixed temperature, while varying the accelerating voltage, since the quality of the diffraction pattern is not too seriously affected by small changes in the voltage. The CB configuration, however, requires precise electron-optical conditions, and the detailed appearance of the CB diffraction patterns is extremely sensitive to changes in the voltage. Direct comparison between consecutive diffraction patterns obtained in this way was found to be invalidated by the continual need to reset focus and other conditions. If, however, the initial electron optical conditions are maintained, the V_c effect may be induced by slowly changing the specimen temperature, hence altering the value of the critical voltage through the Debye–Waller factor. This method was adopted for the experiments reported here. Slow temperature changes ensured that specimen drift was very small, thus consecutive high-quality micrographs could be obtained from substantially the same area of specimen.

4. Theory of the convergent-beam critical-voltage effect

(*a*) *Convergent-beam patterns in thin crystals*

We shall use the Bloch-wave formulation of electron diffraction (Bethe, 1928) and the notation of Humphreys (1979). The total wave function of the incident fast electron within the crystal is represented by a sum of Bloch waves:

$$\psi(\mathbf{r}) = \sum_j \alpha^{(j)} \sum_g C_g^{(j)} \exp[2\pi i(\mathbf{k}^{(j)} + \mathbf{g}).\mathbf{r}] \times \exp(-2\pi \mathbf{q}^{(j)}.\mathbf{r}), \quad (1)$$

where $\mathbf{g}$ is a reciprocal-lattice vector, $\mathbf{k}^{(j)}$ and $\mathbf{q}^{(j)}$ are the real and the imaginary parts, respectively, of the

wave vector of the jth Bloch wave (the imaginary part taking into account phenomenologically the effects of inelastic scattering upon the elastic scattering), $C_g^{(j)}$ is the gth Fourier coefficient of the jth Bloch wave and $\alpha^{(j)}$ is the amplitude of the jth Bloch wave. For the symmetrical Laue case (with **g** parallel to the crystal surface), the electron wave function at the bottom surface of a crystal of thickness t is (*e.g.* Humphreys, 1979)

$$\psi(t) = \sum_j C_0^{(j)*} \sum_g C_g^{(j)} \exp(2\pi i k_z^{(j)} t) \exp(-2\pi q^{(j)} t), \quad (2)$$

where $k_z^{(j)}$ is the component of $\mathbf{k}^{(j)}$ along the normal to the crystal surface. The intensity of the gth diffracted beam is

$$I_g(t) = \left| \sum_j C_0^{(j)*} C_g^{(j)} \exp(2\pi i k_z^{(j)} t) \exp(-2\pi q^{(j)} t) \right|^2. \quad (3)$$

$C_g^{(j)}$, $k_z^{(j)}$ and $\mathrm{q}^{(j)}$ are all functions of the orientation of the crystal relative to the incident beam, *i.e.* they are functions of k_t, where k_t is the tangential component of **k** (*i.e.* in the plane of the crystal surface). Their values are found by substituting (1) into the Schrödinger equation in the usual manner. Hence diffracted beam intensities may be calculated from (3) and these are a function of the angle of incidence of the electron beam. A convergent-beam disc corresponding to a reflection **g** is an intensity map of $I_g(t)$ as a function of k_t, and hence the intensity distribution in a CB disc can be calculated by successive evaluations of (3) for different values of k_t, as was done for the plots of Fig. 2.

For accurate structure-factor determinations using CBED, very thin specimens have been used in previous work for two reasons. Firstly, the accuracy with which the $q^{(j)}$ are known is poor, probably being to no better than 10% (see Humphreys & Hirsch, 1968). Hence, errors in calculated values of $I_g(t)$ are minimized if t is small, from (3). Secondly, (3) gives the intensity of the elastically scattered electrons only. As t increases, an increasing proportion of electrons within the convergent-beam discs are inelastically scattered electrons, the absolute intensity of which is not known accurately (see §4*c*).

(*b*) *The critical-voltage effect*

At any voltage the intensity of a second-order reflection is, from (3)

$$I_{2g}(t) = \left| \sum_j C_0^{(j)*} C_{2g}^{(j)} \exp(2\pi i k_z^{(j)} t) \exp(-2\pi q^{(j)} t) \right|^2. \quad (4)$$

For a crystal set at the second-order reflecting position, Bloch waves 2 and 3 normally have the largest excitation amplitudes (*i.e.* largest values of $C_0^{(j)*}$), and wave 1 is the next largest. The excitations of all other waves are very small. Also waves 2 and 3 are usually the least-absorbed waves, wave 1 being the most strongly absorbed. Equation (4) can therefore be written in the form

$$I_{2g}(t) = \left| \sum_{j=2,3} C_0^{(j)*} C_{2g}^{(j)} \exp(2\pi i k_z^{(j)} t) \times \exp(-2\pi q^{(j)} t) + \Delta \right|^2, \quad (5)$$

where Δ represents the contribution of all waves other than 2 and 3. Because of anomalous absorption Δ is very small for reasonably thick crystals.

At the critical voltage, due to relativistic changes in mass and wavelength of the electrons, there is an accidental degeneracy of Bloch waves 2 and 3, *i.e.* at V_c

$$k_z^{(2)} = k_z^{(3)}, \quad \text{also} \quad C_0^{(2)} C_{2g}^{(2)} \simeq -C_0^{(3)} C_{2g}^{(3)} \quad \text{and} \quad q^{(2)} \simeq q^{(3)}. \quad (6)$$

Hence, from (5) and (6), waves (2) and (3) interfere destructively and $I_{2g}(t)$ is very small, provided that Δ is very small, *i.e.* provided that t is reasonably large. It is important to note that for accurate quantitative CBED work t must be small whereas for accurate critical-voltage work t must be reasonably large (see Lally, Humphreys, Metherell & Fisher, 1972).

(*c*) *Kikuchi patterns from thick crystals*

The most accurate conventional method of determining the critical voltage is by observing the minimizing and asymmetry reversal of Kikuchi lines which occur at the critical voltage. By applying the reciprocity theorem to thick crystals, Thomas & Humphreys (1970) showed that Kikuchi-line intensities could be calculated by summing the rocking-curve intensities at each deviation from the Bragg position. A simple equivalent procedure is to sum the independent Bloch-wave intensities (averaged over a unit cell) at the bottom of the crystal and plot the result as a function of the deviation. Thus the Kikuchi-line intensity is given by

$$I(z) = \sum_j I_g^{(j)} = \sum_j |C_0^{(j)}|^2 \exp(-4\pi q^{(j)} z). \quad (7)$$

Equation (7) applies to symmetrical Kikuchi patterns with the incident beam parallel to the diffracting planes. For asymmetrical Kikuchi patterns, it is necessary to assume that the diffuse scattering is peaked in the primary beam direction, so that each of the component rocking-beam intensities is weighted (Thomas, 1972). Fig. 3 shows calculated Kikuchi profiles, in which the asymmetry change on passing through V_c is clear.

5. Experimental results and their interpretation

(*a*) *Introduction*

Experimentally, the critical-voltage effect, when induced by changing the temperature (or voltage),

causes a characteristic fringe pattern to appear within the CB diffraction disc over a quite narrow range of temperature. This behaviour, however, is not observed if too thin an area of the specimen is examined. In the following, therefore, general features of the variation of the pattern with both temperature and thickness will initially be discussed, with reference to the experimental patterns of Fig. 1. Comparison will then be made with computed patterns, calculated by the methods of § 4. Only the Bragg-satisfied 222 CB diffraction disc will be considered in this section. As we shall see, the most sensitive identification of the temperature at which the degeneracy occurs, the 'critical-voltage temperature' T_{cv}, requires a detailed analysis, taking account of both elastic and diffuse scattering. This is discussed in § 5(*d*). An experimental illustration of the perturbing effects of non-systematic interactions on the fringe pattern is given in § 5(*e*).

Our claim for the equivalence of inducing the critical-voltage effect by changing the temperature, instead of the usual method of changing the voltage, is based upon the linearity of the change in V_c with temperature over a wide range of temperatures, as shown by Lally, Humphreys, Metherell & Fisher (1972). In the present work we use the result given by Hewat (1975) for copper that $dV_c/dT = -0{\cdot}35$ kV K^{-1}.

(*b*) *General features of CB diffraction patterns near* T_{cv}

Far from the temperature, or voltage, at which the degeneracy occurs, the appearance of the satisfied 222 disc, and of the other low-order discs of the systematic row, is as shown in Fig. 1(*a*). As the temperature (or voltage) is varied toward and through the critical value,

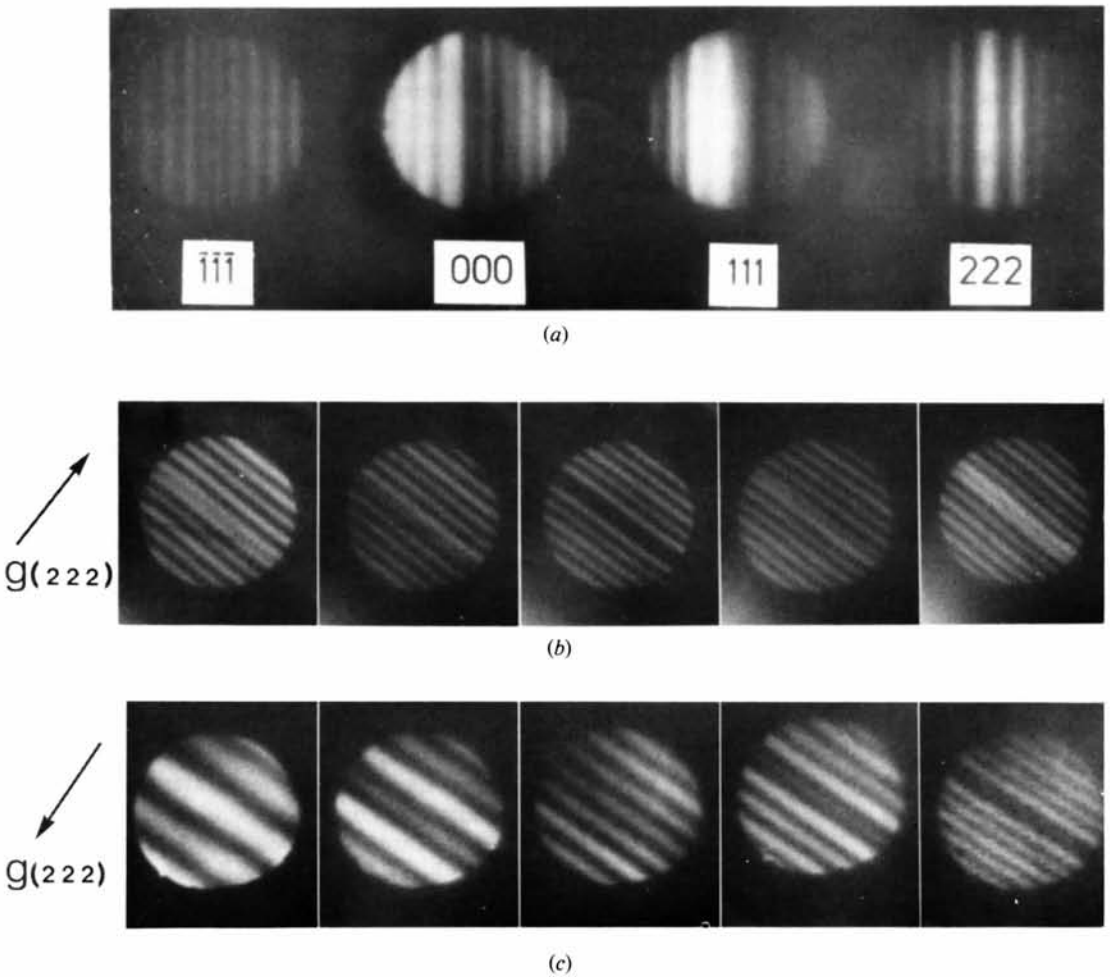

(*a*)

(*b*)

(*c*)

Fig. 1. (*a*) A typical systematic row of convergent-beam discs at a high accelerating voltage, far from V_c; the crystal is set at the 222 Bragg position. (*b*) 222 discs in a thick specimen near the critical voltage. The critical-voltage effect has been induced by changing the temperature. On the left, higher temperatures ($V_c <$ accelerating voltage, V); in the centre $V_c \simeq V$, note the characteristic 'dark-band' feature; on the right, lower temperatures ($V_c > V$). (*c*) The appearance of the 222 disc, when $V_c \simeq V$, for values of the specimen thickness increasing from the left. In thinner areas there is no 'dark band' and the critical voltage cannot be easily identified.

the intensity of the Bragg peak passes through a minimum. For a sufficiently thick area of a specimen, this results in a striking visual effect within the disc. A 'dark band' appears in the fringe pattern, as illustrated by the series of patterns shown in Fig. 1(*b*). In such thick areas, increasing the thickness further decreases the fringe spacing, but has little effect on the general appearance of the fringes. Fig. 1(*c*) illustrates, however, that thinner areas exhibit wide variations in the form of the fringe pattern, without any suggestion of a 'dark band' at temperatures near T_{cv}. Therefore, quite thick areas are required for CB critical-voltage experiments but, in practice, the reduction of intensity with increasing thickness, and the available angular resolution, limit the useful range of thickness.

The 'dark-band' feature is visible over a range of temperatures corresponding to a spread in accelerating voltage of some 20 kV. This corresponds quite closely to the region within which loss of detail in, for example, Kikuchi-line patterns has been responsible for the observational error quoted in previous V_c determinations. The ability of the convergent-beam technique to yield detailed information within this region is the basis of our claim to greatly increased observational sensitivity.

(*c*) *Comparison with calculated CB patterns*

Fig. 2 shows a number of rocking curves, calculated using (3), for the Bragg-satisfied 222 reflection in copper. In the calculations ξ_{111} is taken from Hewat (1975), ξ_{222} from Wakoh & Yamashita (1971) and all higher-order extinction distances from Doyle & Turner (1968). Absorption coefficients are taken from Humphreys & Hirsch (1968). The Debye–Waller parameter B was calculated to be 0·643 at T_{cv} as measured in pure copper (see § 6). For this combination of parameters the calculated critical voltage is 305 kV.

The main conclusions to be drawn from the calculated rocking curves are: (i) the curves are symmetric about the reflecting position; (ii) there is a sharply defined intensity minimum at the exact Bragg position which approaches zero for thick specimens at T_{cv} (or V_c). Averaging due to the limited angular resolution then accentuates the low average intensity

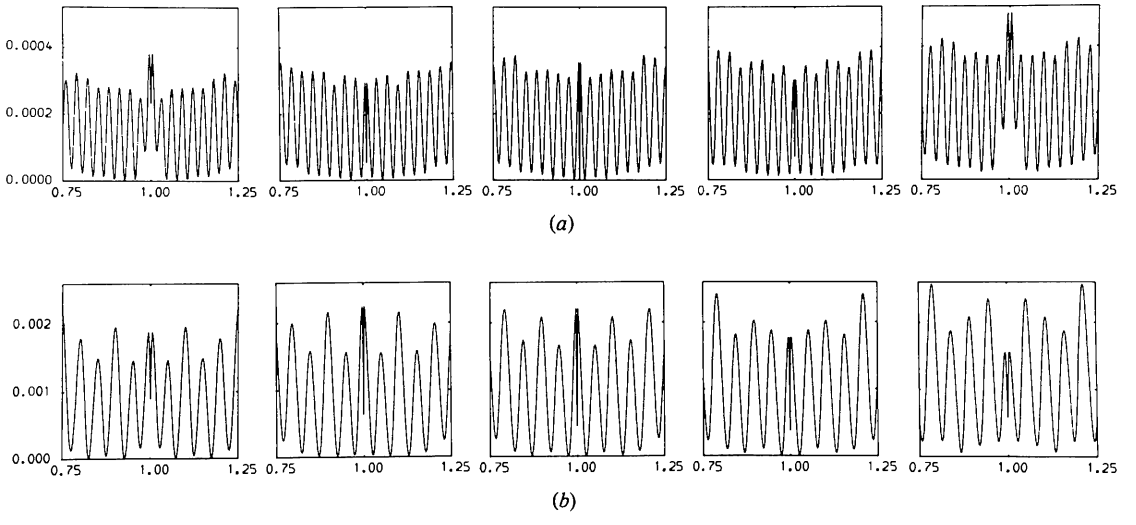

Fig. 2. Calculated elastically scattered intensity profiles (rocking curves) corresponding to the Bragg-satisfied 222 CB disc in copper. In both (*a*) and (*b*) the value of the accelerating voltage used in each calculation has been increased, from the left. The values are 290, 300, 305 ($=V_c$), 310 and 320 kV. Sequence (*a*) is for a foil thickness $15\xi_{111}$ (≃4500 Å) and (*b*) is for a thickness $9\xi_{111}$ (≃2700 Å). Note that in (*b*) the foil is insufficiently thick to identify the critical voltage.

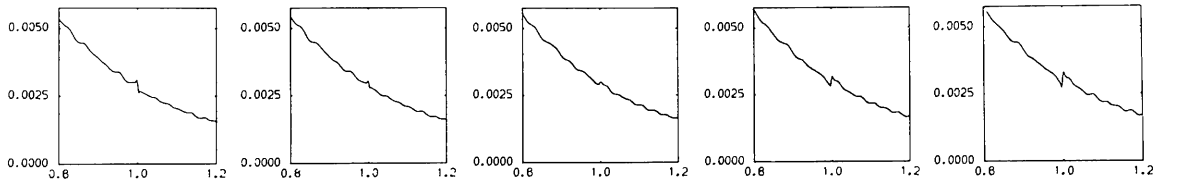

Fig. 3. Calculated inelastically scattered electron contributions to the Bragg-satisfied 222 CB disc in copper for accelerating voltages 300 (left), 302, 305 ($=V_c$), 308, 310 kV (right). Note the asymmetric decreasing intensity across the disc and the reversal of asymmetry of the Kikuchi line on passing through V_c.

near the reflecting position, resulting in the 'dark-band' contrast; (iii) in thin specimens the contrast of this minimum is poor, and there is considerable intensity in the two central peaks on either side, with the result that no 'dark band' will be seen; (iv) the number of intensity peaks increases with the specimen thickness, and the peaks become approximately sinusoidal away from the centre of the pattern.

These points can be simply explained. Point (i) is a consequence of the reciprocity theorem (see Pogany & Turner, 1968). Points (ii) and (iii) follow from (5) and (6) and § 4(*b*). Point (iv) can be explained by noting that at the critical voltage, for small deviations s from the second-order Bragg position, $k_z^{(2)} - k_z^{(3)}$ varies linearly with s, *i.e.* $k_z^{(2)} - k_z^{(3)} = Cs$ (Hewat, 1975), where C is a dimensionless constant. Also, for small s and at V_c, it is still approximately true that $q^{(2)} \simeq q^{(3)}$ and $C_0^{(2)} C_{2g}^{(2)} \simeq -C_0^{(3)} C_{2g}^{(3)}$. Hence (5) yields that the intensity peaks are of the form $\sin^2(\pi Cst)$, instead of the usual shape-transform type, of the form $|(\sin \pi ts')/\pi s'|^2$, [where $s' = (s^2 + \xi_g^{-2})^{1/2}$], obtained far from V_c (*cf.* Fig. 1*a* for example).

Microdensitometer traces of experimental 222 CB discs (Fig. 5) display an asymmetric, decreasing average intensity across the disc, whereas the calculated profiles of Fig. 2 are symmetric. The reason for this apparent discrepancy is that the intensity in CB discs using thick specimens is due to contributions from both elastically and inelastically scattered electrons. Thus to calculate such CB discs, Kikuchi-line profiles, calculated as described in § 4(*c*), must be added to the calculated intensities of Fig. 2. Examples of the calculated inelastic contribution to the 222 disc intensity for a thick specimen are shown in Fig. 3. The inelastically scattered contribution consists of a slowly and almost linearly varying background with sharp, asymmetric Kikuchi lines. Where the degeneracy occurs, the Kikuchi line changes asymmetry and shows minimum contrast.

(*d*) *Precise determination of* T_{cv}

Fig. 4 shows the variation in the 222 CB disc for Cu 5% Al as the temperature is varied from that at which the 'dark band' first becomes evident, to a temperature very near T_{cv}. The sharp central-peak extinction effect predicted by calculated elastic-scattering profiles (Fig. 2) is blurred experimentally by insufficiently high angular resolution and also by inelastic diffuse scattering. However, the very low, averaged, elastically scattered intensity in the 'dark-band' region allows the asymmetry of the Kikuchi line to be clearly distinguished, so that T_{cv} may be identified using the criterion of vanishing asymmetry. The asymmetry may be studied in detail at temperatures near T_{cv} by the use of microdensitometer traces taken across the discs. For example, Fig. 5 shows a composite of traces from three consecutive patterns separated from each other by 9 K in temperature (*i.e.* equivalent to 3 kV separation in voltage) using a Cu–5% Al specimen. The middle trace (*i.e.* Fig. 5*b*) most nearly satisfies the T_{cv} criterion of symmetry with respect to the background. Based on the sensitivity evident in the traces of Fig. 5 even the crudest interpolation scheme would indicate that an experimental discrimination of T_{cv} to within ± 3 K (*i.e.* ± 1 kV in V_c) is justified.

As noted earlier, for a crystal set at the 222 Bragg position, the calculated 222 CB disc is symmetrical for the elastically scattered electrons (Fig. 2). However, the calculated inelastic scattering contribution to the disc is asymmetrical (Fig. 3), and hence the total intensity distribution across the disc is asymmetrical (Fig. 5). The contribution of inelastically scattered electrons to the disc consists of two parts, an asymmetric slowly varying 'background' intensity and an asymmetric rapidly varying Kikuchi line (see Fig. 3). At the critical voltage the Kikuchi line vanishes. It is instructive to attempt a subtraction of the inelastic 'background' intensity from experimental CB patterns. If our interpretation is correct, such a subtraction from an experimental 222 CB disc observed at the critical voltage should give the symmetrical intensity distribution due to essentially elastic scattering. Away from the critical voltage, subtracting the inelastic background should give the symmetric elastic distribution with the asymmetric Kikuchi line superimposed. A crude background subtraction may be carried out by using a linear approximation to the background, as suggested by the profiles of Fig. 3. Fig. 6(*a*) displays the result given by this procedure when applied to the trace at T_{cv} shown in Fig. 5(*b*), with

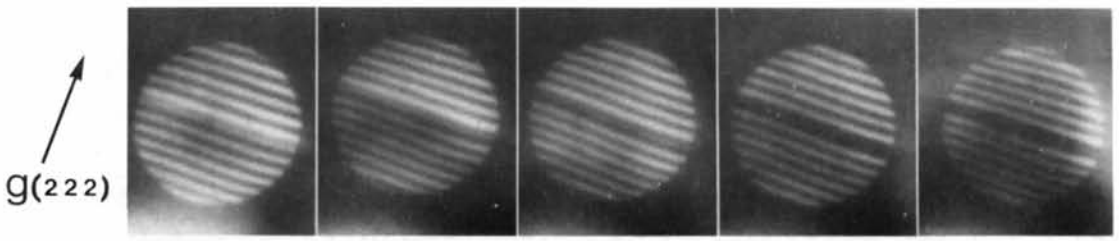

Fig. 4. The appearance of the 222 CB disc in Cu–5% Al as, from the left, the specimen temperature is decreased in 12 K (=4 kV change in V_c) steps until, on the right, V_c has increased to a value equal to the accelerating voltage.

which it should be compared. The procedure, demonstrating essentially the variation of the elastically scattered intensity, has also been applied to a trace of another experimental pattern, obtained in a separate T_{cv} determination on Cu–5% Al in which a thicker area was examined. The result is given in Fig. 6(*b*). Both 'corrected' traces demonstrate very clearly the absence of asymmetry at the reflecting position, which would still remain after subtraction at a temperature away from T_{cv}. These traces also show good agreement with the computed elastic-scattering fringe profiles of Fig. 2, and the theoretical analysis of § 4. In particular: (i) the subsidiary maxima are symmetric about the reflection position, and are sinusoidal in the trace from the thicker area; (ii) in the thinner area, an additional intensity component is observed with periodicity twice that of the sinusoidal fringes in both experimental and computed fringe profiles, attributable to the beating between Bloch waves 1 and 2; (iii) the incomplete absorption of Bloch wave 1 also accounts for the remaining averaged intensity in the 'dark-band' region, in the thinner area.

(e) The effect of the excitation of non-systematic reflections

The convergent-beam method enables a clear visual picture of the effects of non-systematic reflections to be obtained, and an estimate of their importance. Fig. 7 shows two examples, in which both discs are seen to be traversed by Kikuchi lines. There is little visible effect on the fringe pattern in (*a*), and a very strong effect in (*b*). Densitometer traces taken across perturbed discs indicated that the value of T_{cv} was detectably altered only in a region close to the Kikuchi line in a situation such as that represented in Fig. 7(*a*). It is therefore not difficult to minimize the effects of such accidental reflections experimentally.

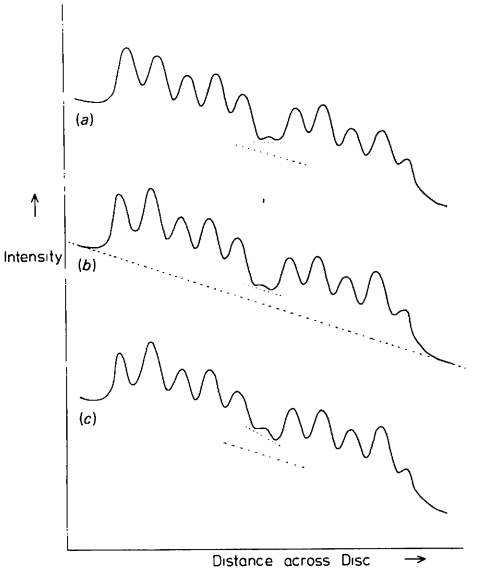

Fig. 5. Each microdensitometer trace shows the variation of intensity diametrically across an experimental 222 CB disc fringe pattern, normal to the fringes (*i.e.* in the direction of **g**). (*a*), (*b*) and (*c*) are 9 K apart in the specimen temperature (≡3 kV in V_c value). The lack of asymmetry of the 'dark band' in (*b*) relative to the background (dotted line) indicates that V_c is very close to the accelerating voltage for this case.

6. Application to the determination of scattering factors

Determination of the first-order scattering factor f_{111} (proportional to V_{111}) by comparing the single result of a critical-voltage measurement with *n*-beam dynamical calculations necessitates the assumption of values for the other scattering factors, for example from the tabulations of Doyle & Turner (1968). For a low-index reflection such as the 222 reflection in copper, percentage errors in the value of f_{222} are more important than uncertainties in the temperature, whilst errors in f_{333} are an order of magnitude less important. Dividing the proportional error in f_{111} into three separate contributions – due to proportional errors in f_{222}, the Debye–Waller factor B, and the critical voltage V_c – it is found, using a three-beam expression for the relation between the first two effective scattering factors at V_c, that

$$\frac{\delta f_{111}}{f_{111}} = 0{\cdot}6\,\frac{\delta f_{222}}{f_{222}} + 0{\cdot}1\,\frac{\delta B}{B} + 0{\cdot}2\,\frac{\delta V_c}{V_c}.$$

Each of these contributions may be examined separately:

(i) $\delta f_{222}/f_{222}$. Detailed comparison of calculated rocking curves with the experimental CB discs of a

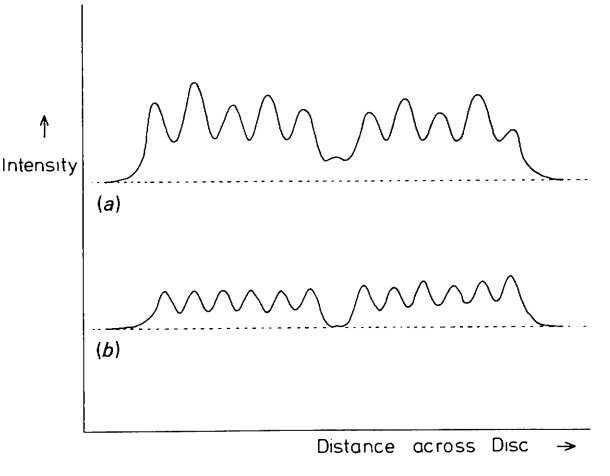

Fig. 6. Intensity profiles after subtraction of a linearly varying background component. (*a*) corresponds to the microdensitometer trace of Fig. 5(*b*) and (*b*) shows a similarly obtained profile, but for a thicker specimen. For discussion see text.

systematic row should permit a refinement of f_{222} to 1% accuracy.

(ii) $\delta B/B$. This depends on the accuracy of specimen-temperature measurement and with which the Debye temperature is known. With care, and in the favourable case of copper specimens, the total error is thought to approach 4%, and may be reduced slightly by measuring T_{cv} at two or more voltage settings.

(iii) $\delta V_c/V_c$. In previous work this has been the largest contribution to the error in f_{111} due to large observational errors in V_c measurement. As demonstrated in § 5, the observational error has been reduced to the ± 1 kV level, comparable in magnitude to the error introduced by uncertainty in the exact value of the accelerating voltage (this may be measured using the technique due to Høier (1969) to ± 1 kV for copper near 300 kV) and uncertainty in V_c due to non-systematic interactions (repeated experiments indicate reproducibility to within ± 1 kV). Reducing the observational error further would therefore not improve the accuracy to which f_{111} can be determined.

The following results were obtained from repeated experiments on pure copper. At an accelerating voltage of 305 ± 1 kV (measured using the technique due to Høier, 1969) the critical-voltage effect occurred at a temperature measured to be 356 ± 5 K. Unfortunately, some uncertainty in the value of systematic errors in the temperature measurement (a thermocouple attached to the hot stage was used) prevents us from giving a full discussion of the derivation of a value for f_{111}. However, the value calculated for V_c at this temperature was also 305 kV, using ξ_{111} taken from Hewat (1975) (see § 5*c*). If the temperature measurement is accepted, therefore, we obtain the same value for f_{111} as Hewat (1975), but with reduced errors.

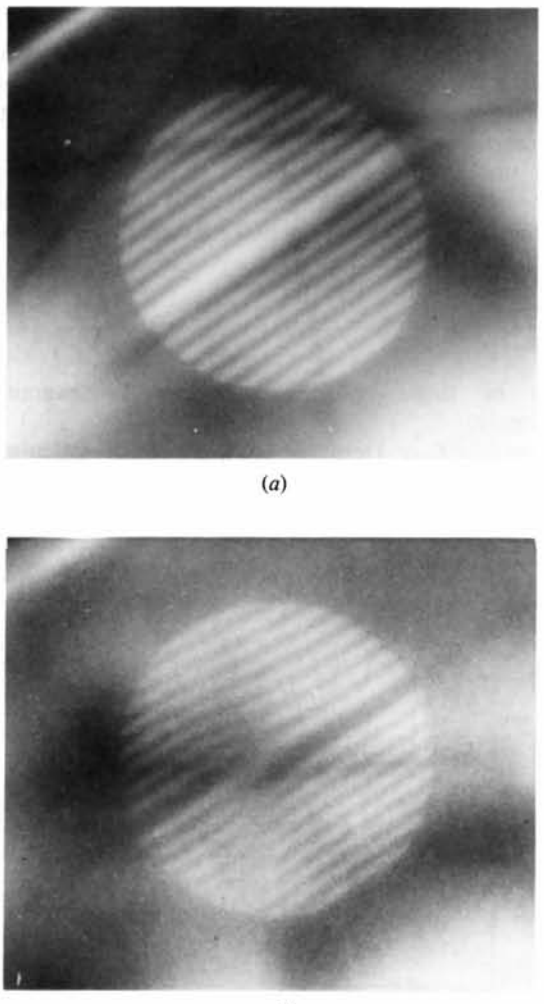

(*a*)

(*b*)

Fig. 7. The strength of a non-systematic interaction may easily be judged from the CB fringe pattern, which can be unaffected (*a*), or highly perturbed (*b*).

7. Application to the study of alloys

It could be argued that a method with such sensitivity might be useful in detecting small changes in the value of T_{cv}, or V_c, due to a redistribution of scattering power in the crystal. Such changes occur when, for example, solute atoms are introduced or change their internal arrangement as in a change from an ordered to a disordered state. Previous attempts to utilize V_c measurements in the detection of short-range order (SRO) in alloys have met with only limited success, due to the relatively large uncertainty (± 5 kV or more) in measured V_c values (*e.g.* Sinclair, Goringe & Thomas, 1975; Kuroda, Tomokiyo & Eguchi, 1977, 1978). In this section an investigation using α-CuAl alloys of varying concentration is reported; in particular, it was thought the change might be detected from the purely random solute distribution in the more dilute alloys, to a partly ordered distribution in the more concentrated alloys, by following the change in T_{cv} with aluminium concentration. Recent calculations (Shirley & Fisher, 1979), based on a statistical theory of ordering (Shirley, 1974), indicate a V_c (222) difference of up to 5 kV between random and partly ordered states in the more concentrated α-CuAl alloys, thought to be detectable by this method, but not by other methods. The temperature-varying method may be used as long as T_{cv} is well below the temperatures at which rapid changes in order occur. For the concentrated CuAl alloys rapid changes occur above approximately 473 K (*e.g.* Matsuo & Clarebrough, 1963; Trieb & Veith, 1978).

The degree of SRO makes a considerable difference to the static component of the atomic displacements due to the microscopic strains introduced into the alloy by the effective atomic-radius disparity between the

components (size effect). Shirley & Fisher (1979) have utilized a wide range of critical-voltage data to test the validity of a two-parameter model for the atomic displacements in cubic binary alloys which, when used in conjunction with *n*-beam dynamical computations, yields V_c values as functions of composition, temperature and SRO. Briefly, the theory involves two fitted parameters, τ and γ. τ represents the degree of difference in the force constants operating between the two components of the alloy and the arithmetical mean of the constants for each taken singly. γ connects static displacement-correlation functions with alloy constitutive constants, order parameters and the variation of the lattice constant with composition. Both γ and τ are of order unity and should vary only a little with composition for a given binary alloy.

Fig. 8 shows T_{cv} values in pure copper and the three CuAl alloys as a function of aluminium concentration, for a constant accelerating voltage (305 kV). The value shown for pure copper is *not* our measured value, but is that calculated using scattering-factor data, Debye temperatures and lattice-spacing data set out in Thomas, Shirley, Lally & Fisher (1974). The values for the CuAl alloys are obtained from the differences measured in our experiments between T_{cv} in each alloy and in pure copper (and hence their error bars are augmented by the error in the determination of the result in pure copper). This procedure allows estimates of γ and τ to be obtained from the computations of Shirley & Fisher (1978). Fitting to the result for Cu–5% Al, in which it is thought there is little or no SRO (Epperson, Fürnrohr & Ortiz, 1978), gives

$$\tau = 1{\cdot}00 \pm 0{\cdot}24, \quad \gamma = 2{\cdot}05 \pm 0{\cdot}30.$$

Knowledge of these parameters allows the prediction of T_{cv} values for alloys of other solute concentrations. In Fig. 8, the full line represents the theoretically predicted values of T_{cv} as a function of aluminium concentration with $\tau = 1{\cdot}00$ and $\gamma = 2{\cdot}05$, assuming no SRO. The dotted lines on either side represent limits on the allowed predicted values due to the stated errors in the determination of τ and γ. The measured values for Cu–11·5% Al and Cu–16·73% Al both appear to be consistent with those expected if SRO were not present in these particular specimens, lying within the rather large range of values predicted using the present estimates of τ and γ.

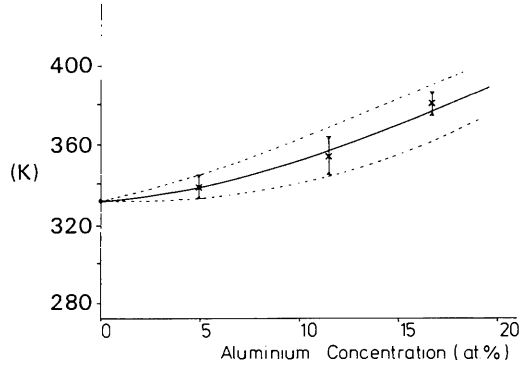

Fig. 8. Variation of T_{cv} with aluminium concentration in CuAl alloys. The solid curve shows the computed result with $\gamma = 2{\cdot}05$, $\tau = 1{\cdot}00$, and the dashed curves give the variation consistent with fitting γ, τ to the extremes of the Cu–5% Al experimental result. The experimental results for the higher alloys (crosses with error bars) do not show significant deviation from the results expected with these values of γ and τ.

Considering how small a change by SRO is theoretically predicted for these alloys, the failure to detect SRO experimentally reflects the accumulation of errors by compounding those from separate measurements, rather than insensitivity in individual T_{cv} determinations. A better method might use a single alloy, changing the state of order by annealing and rapid-quenching treatments and then searching for a change in T_{cv}. However, recent work suggests that the order structure may be a hybrid containing both SRO and poorly developed LRO in small domains (Epperson, Fürnrohr & Ortiz, 1978). This will partly relieve the size-effect strains, leading to an even smaller difference in T_{cv} or V_c values, precluding their detection in this particular alloy system.

8. Summary and conclusions

1. Following the preliminary results of Moodie, Sellar, Imeson & Humphreys (1977) and Moodie, Humphreys, Imeson & Sellar (1978), the critical-voltage effect and the convergent-beam electron diffraction technique have been combined in a single experiment and the results interpreted in detail.

2. The new method yields an accuracy in V_c determination of ± 1 kV compared with ± 5 kV available with previous methods.

3. The critical voltage has been determined by varying the specimen temperature at constant voltage rather than varying the voltage at constant temperature. This new method has the advantage that all the electron-optical parameters are kept constant.

4. A characteristic 'dark band' appears in the Bragg-satisfied second-order CB disc near the critical voltage V_c (or the critical-voltage temperature T_{cv}). This enables the critical voltage to be approximately located very easily. It is however necessary to use sufficiently thick specimens for the dark band to be clearly displayed.

5. Because thick areas must be used, the intensity in the CB discs contains contributions from elastically and inelastically scattered electrons. The latter may be divided into a slowly varying (in angle) 'background' and the rapidly varying Kikuchi line.

6. Changes in the asymmetry of the Kikuchi line within the dark band enable an observational

localization of V_c to ± 1 kV to be made (or, equivalently for copper, T_{cv} to ± 3 K).

7. The improved precision of the new method considerably increases its application to the accurate determination of low-order scattering factors in pure materials, and also to ordering and electron transfer in certain alloys. This method has been illustrated by applying it to Cu and Cu–Al alloys.

8. Development of the technique involves improving the angular resolution within the convergent-beam diffraction disc. Further reduction in the spot size, better electron-optical performance, or the use of materials with greater structural rigidity, might achieve this.

The authors are very grateful to Dr C. G. Shirley for discussions, Mr D. A. Smart for his help with computing, Mr R. Doole for assistance with the high-voltage electron microscope, Professor Sir Peter Hirsch FRS for providing laboratory facilities and the Science Research Council for financial support.

References

ARII, A., UYEDA, R., TERASAKI, O. & WATANABE, D. (1973). *Acta Cryst.* A**29**, 295–298.

BELL, W. (1971). In *Proc. 29th Ann. EMSA Meeting*, edited by C. ARCENEAUX, pp. 184–185. Baton Rouge: Claitors.

BETHE, H. A. (1928). *Ann. Phys. (Leipzig)*, **87**, 55–129.

BUTLER, P. (1972). *Philos. Mag.* **26**, 33–41.

BUTLER, P. (1973). *Phys. Status Solidi A*, **18**, 71–83.

COWLEY, J. M. (1978). *Adv. Electron. Electron Phys.* **46**, 1–53.

DOYLE, P. A. & TURNER, P. S. (1968). *Acta Cryst.* A**24**, 390–397.

EPPERSON, J. E., FÜRNROHR, P. & ORTIZ, C. (1978). *Acta Cryst.* A**34**, 667–681.

GOODMAN, P. (1976). *Acta Cryst.* A**32**, 793–798.

GOODMAN, P. (1978). *Electron Diffraction* 1927–1977, edited by P. J. DOBSON, J. B. PENDRY & C. J. HUMPHREYS, *Inst. Phys. Conf. Ser.* **41**, 116–128.

GOODMAN, P. & LEHMPFUHL, G. (1967). *Acta Cryst.* **22**, 14–24.

HEWAT, E. A. (1975). D.Phil. Thesis, Univ. of Oxford.

HEWAT, E. A. & HUMPHREYS, C. J. (1974). *High-Voltage Electron Microscopy*, edited by P. R. SWANN, C. J. HUMPHREYS & M. J. GORINGE, pp. 52–56. New York: Academic Press.

HØIER, R. (1969). *Acta Cryst.* A**25**, 516–518.

HUMPHREYS, C. J. (1979). *Rep. Prog. Phys.* **42**, 1825.

HUMPHREYS, C. J. & HIRSCH, P. B. (1968) *Philos. Mag.* **18**, 115–122.

KURODA, K., TOMOKIYO, Y. & EGUCHI, T. (1977). *J. Electron Microsc. Suppl.* **26**, 259–262.

KURODA, K., TOMOKIYO, Y. & EGUCHI, T. (1978). *Proc. Ninth Int. Conf. Electron Microsc., Toronto*, edited by J. M. STURGESS, Vol. 1, pp. 192–193.

LALLY, J. S., HUMPHREYS, C. J., METHERELL, A. J. F. & FISHER, R. M. (1972). *Philos. Mag.* **25**, 321–343.

LEHMPFUHL, G. (1978). *Proc. Ninth Int. Conf. Electron Microsc., Toronto*, edited by J. M. STURGESS, Vol. 3, pp. 304–315.

MATSUO, S. & CLAREBROUGH, L. M. (1963). *Acta Metall.* **11**, 1195.

MOODIE, A. F., HUMPHREYS, C. J., IMESON, D. & SELLAR, J. R. (1978). *Electron Diffraction* 1927–1977, edited by P. J. DOBSON, J. B. PENDRY & C. J. HUMPHREYS, *Inst. Phys. Conf. Ser.* **41**, 129–134.

MOODIE, A. F., SELLAR, J. R., IMESON, D. & HUMPHREYS, C. J. (1977). *J. Electron Microsc. Suppl.* **26**, 191–194.

NAGATA, F. & FUKUHARA, A. (1967). *Jpn. J. Appl. Phys.* **6**, 1233–1241.

POGANY, A. P. & TURNER, P. J. (1968). *Acta Cryst.* A**24**, 103–109.

RACKHAM, G. M. & RICKARDS, G. K. (1977). *Optik*, **47**, 223–226.

SHIRLEY, C. G. (1974). *Phys. Rev. B*, **10**, 1149–1159.

SHIRLEY, C. G. & FISHER, R. M. (1978). Private communication.

SHIRLEY, C. G. & FISHER, R. M. (1979). *Philos. Mag.* **39**, 91–117.

SHISHIDO, T. & TANAKA, M. (1976). *Phys. Status Solidi*, **38**, 453–461.

SINCLAIR, R., GORINGE, M. J. & THOMAS, G. (1975). *Philos. Mag.* **32**, 501–512.

SMART, D. J. & HUMPHREYS, C. J. (1978). *Electron Diffraction* 1927–1977, edited by P. J. DOBSON, J. B. PENDRY & C. J. HUMPHREYS, *Inst. Phys. Conf. Ser.* **41**, 145–149.

SMITH, D. J. & COWLEY, J. M. (1971). *J. Appl. Cryst.* **4**, 482–489.

STEEDS, J. W., JONES, P. M., RACKHAM, G. M. & SHANNON, M. D. (1976). In *Developments in Electron Microscopy and Analysis*, edited by J. A. VENABLES, pp. 351–356. London, New York: Academic Press.

THOMAS, L. E. (1972). *Philos. Mag.* **26**, 1447–1465.

THOMAS, L. E. & HUMPHREYS, C. J. (1970). *Phys. Status Solidi*, **3**, 599–615.

THOMAS, L. E., SHIRLEY, C. G., LALLY, J. S. & FISHER, R. M. (1974). *High-Voltage Electron Microscopy*, edited by P. R. SWANN, C. J. HUMPHREYS & M. J. GORINGE, pp. 33–47. New York: Academic Press.

TRIEB, C. & VEITH, G. (1978). *Acta Metall.* **26**, 185–196.

WAKOH, S. & YAMASHITA, J. (1971). *J. Phys. Soc. Jpn*, **30**, 422–427.

WATANABE, D., UYEDA, R. & KOGISO, M. (1968). *Acta Cryst.* A**24**, 249–250.